Electronic Supplementary Material (ESI) for Journal of Materials Chemistry C.


# Broad-Band Emission in All-Inorganic Metal Halide Perovskite with Intrinsic Vacancies

Feng Jiang[a,b,#], Xingxing Jiang [a,#], Weihao Zheng[c], Yu Ouyang [a,b], Yushuang Zhang[c], Lihui Li [a,b], Yang Li[a,b], Peng Fan[c], Hepeng Zhao [a,b], Yang Li [a,b], Ying Jiang [a,b], Xiaoli Zhu [a,b], Xiujuan Zhuang [a,b]*, Yexin Feng [a]* & Anlian Pan[c]*

[a]*School of Physics and Electronics, Hunan University, Changsha, Hunan 410082, P. R. China;*
[b]*Key Laboratory for Micro-Nano Physics and Technology of Hunan Province, Hunan University, Changsha, Hunan 410082, P. R. China;*
[c]*Key Laboratory for Micro-Nano Physics and Technology of Hunan Province, College of Materials Science and Engineering, Hunan University, Changsha, Hunan 410082, P. R. China;*

[#]These authors contributed equally.

[*]Emails: zhuangxj@hnu.edu.cn; yexinfeng@pku.edu.cn ;

**I. Material Growth**

The Yb and Er doped perovskite were grown by a chemical vapor deposition method. An alumina boat containing of a mixture of CsX, $PbX_2$ (X= Cl, Br) and $YbCl_3$ ($YbCl_3$·3H2O) (Alfa Aesar, 99.99%) powders was placed at the heating zone. All chemicals were purchased and used without any purification unless otherwise stated. Several pieces of Si substrate were placed at the downstream of the quartz tube to grow the samples. Similar methods are available in previous reports 1 and 2. Before the growth process, the high-purity Ar gas with high flow rate (>500 sccm) was introduced into the system to clean the impurity gas. Then heated the furnance to ~775 ℃ at high speed and keep the temperature for 5~10 minutes. During this procedure, a constant flow of 35 SCCM high-purity Ar gas was introduced as a carrier gas. The CsX and PbX2 was purchased from Xi'an Polymer Light Technology Corp and used without further purification.

**II. Computational Methods** The calculations are performed within the framework of density functional theory (DFT)[3] as implemented in the Vienna Ab initio Simulation Package (VASP)[4]. The generalized gradient approximation (GGA) with Perdew-Burke-Ernzerhof (PBE)[5] was used to describe the exchange-correlation potential. The planewave kinetic-energy cutoff was set to 450 eV. The supercell approach was used to calculate the formation energies of a series of defects, including vacancies and substitutional defects with the 3 × 3 × 3 supercell. We use the 2 × 2 × 2 supercell to calculate the electronic structures. The Brillouin zone was sampled by a 3×3×3 k-mesh for 2×2×2 supercell and a 2×2×2 k-mesh for the 3×3×3 supercell. After the introduction of the vacancy and dopant, all the configurations were fully relaxed. The criterion to terminate the optimization of atomic positions is the force acting on each atom is less than 0.01 eV/Å. The formation energies of the defects in $CsPbCl_2Br$ supercell are calculated as: $E_f = E_{tot(m,n)} - E_{tot(0,0)} - m\mu_{Yb} + m\mu_x + n\mu_v$, where $E_{tot(m,n)}$ is the total energy of the structure containing defect and $E_{tot(0,0)}$ is the total energy of the pristine supercell without defect. m is the number of substituted X (X=Pb, Cs) atoms by Yb atoms, and n is the number of atoms taken out of the supercell to form the vacancy. The symbols $\mu_{Yb}$, $\mu_x$ and $\mu_v$ are the chemical potentials of Yb, X and vacancy atoms, respectively, which were derived from their bulk phase or gas phase.

**III. PL spectra and dynamical measurements** The microware transient PL and the carrier dynamic study of a single MP are performed by a new setup experiment approach. Briefly, a mode-locked Ti:sapphire laser (Tsunami) is pumped by a CW laser at 532 nm (Millennia Prime 10W). The output laser pulse at 800 nm (pulse width of 80 fs, repetition rate of 80 MHz) is introduced to a BBO crystal. The frequency-doubled laser beam at 400 nm is separated from fundamental frequency beam by a dichroic mirror and then aligned to a confocal microscope (Alpha 300 M+ from Witec) with an objective lens (×50) and focuses to a spot with a tunable diameter. The PL is collected by the same objective from the sample then is aligned to the streak camera. The variable-temperature PL measurements were performed using a 50× objective lens with a commercially available liquid $N_2$ cooled stage.

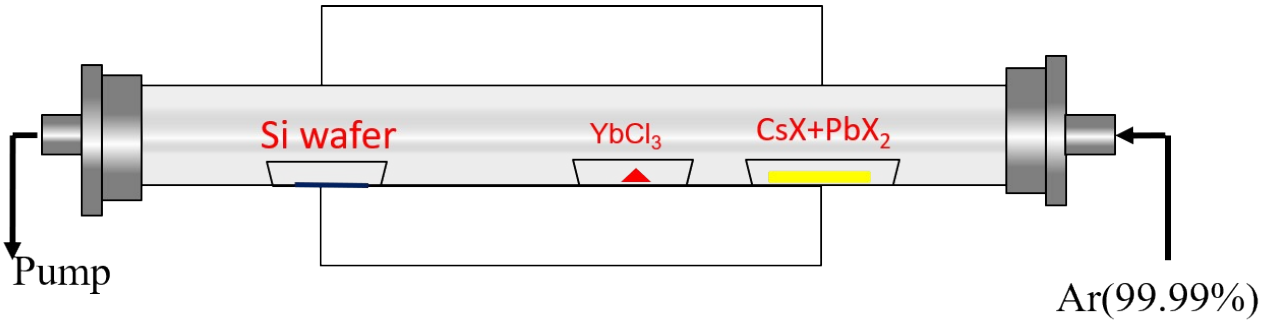


**Figure S1.** Schematic of the setup used for the growth of cesium lead halide perovskite microplates (Yb:$CsPb(Br/Cl)_3$ MPs).

**Table S1.** EDX results of the Yb:$CsPb(Br/Cl)_3$ MPs.

| Element | Weight (%) | Atomic (%) |
|---|---|---|
| Yb | 0.59 | 0.08 |
| Cl | 0.31 | 40.07 |
| Cs | 0.57 | 23.85 |
| Pb | 0.71 | 20.73 |
| Br | 0.40 | 15.27 |

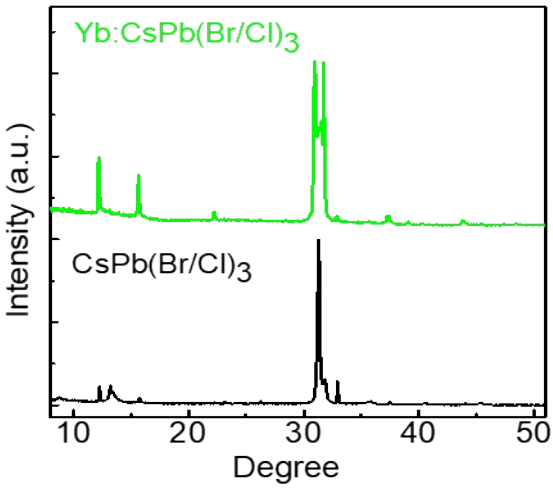


**Figure S2.** Powder XRD patterns from MP with and without Yb doping.

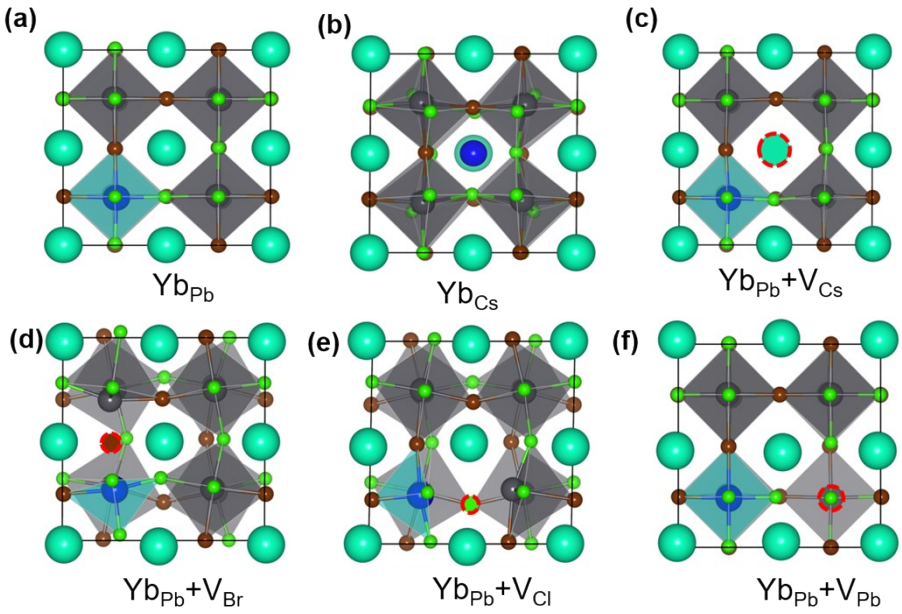


**Figure S3.** (a)-(f) Optimized crystal structure of Yb:$CsPb(Br/Cl)_3$ with and without defects, including vacancy ($V_{Cs}$, $V_{Pb}$, $V_{Cl}$ and $V_{Br}$), substitutional ($Yb_{Pb}$ and $Yb_{Cs}$) and complex defects ($Yb_{Pb}+V_{Cs}$, $Yb_{Pb}+V_{pb}$, $Yb_{Pb}+V_{Cl}$ and $Yb_{Pb}+V_{Br}$). The blue ball represents the substitutional Yb atom ($Yb_{Pb}$ and $Yb_{Cs}$), and the red dotted circle indicates the vacancy ($V_{Cs}$, $V_{Br}$, $V_{Cl}$ and $V_{Pb}$).

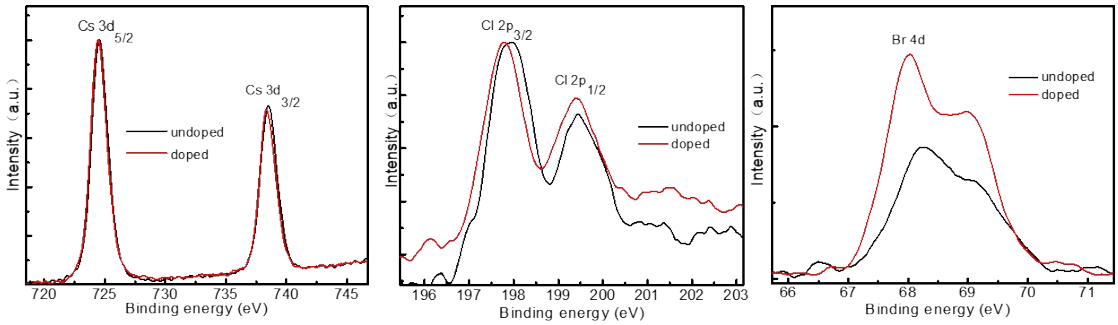


**Figure S4.** The high-resolution XPS analysis corresponding to Cs 3d, Cl 2p and Br 4d, respectively.

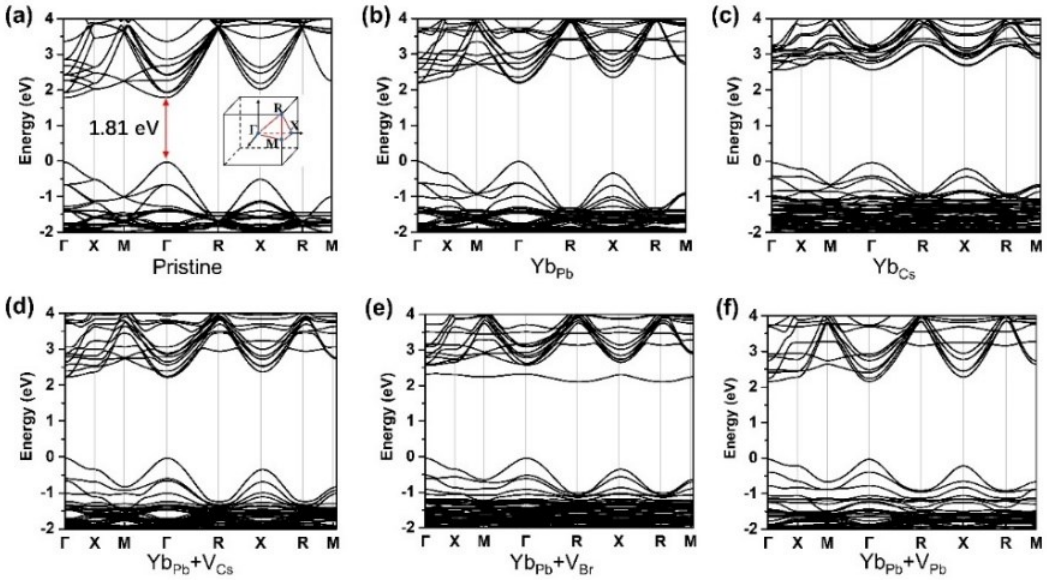


**Figure S5.** (a) Band structure of pristine $CsPb(Br/Cl)_3$. (b)-(f) Band structures of Yb:$CsPb(Br/Cl)_3$ with several kinds of defects.

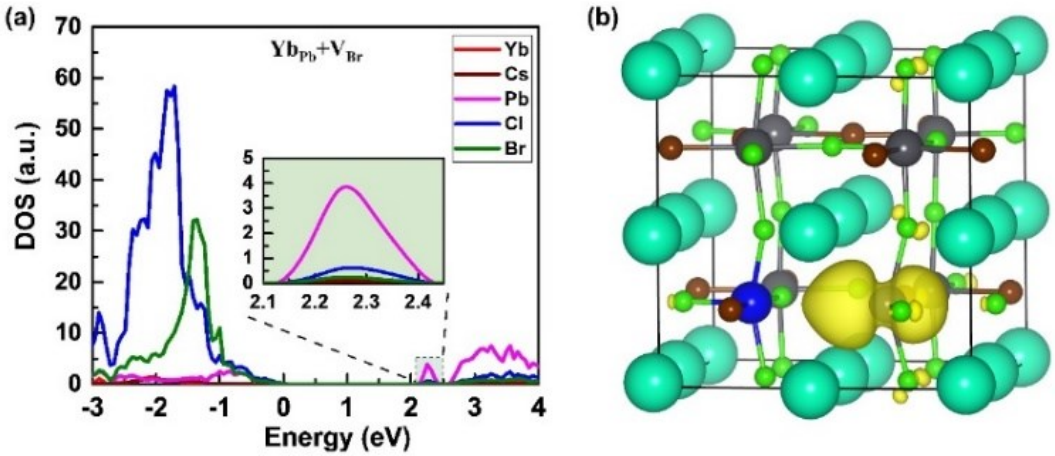


**Figure S6.** (a) DOS of Yb:CsPb(Br/Cl)$_3$ with a Br vacancy. The inset shows that the main contribution of the defect level within the band gap is from the Pb atom. (b) The charge distribution of defect state with isosurface value of 0.0023 eÅ$^{-3}$ (yellow).

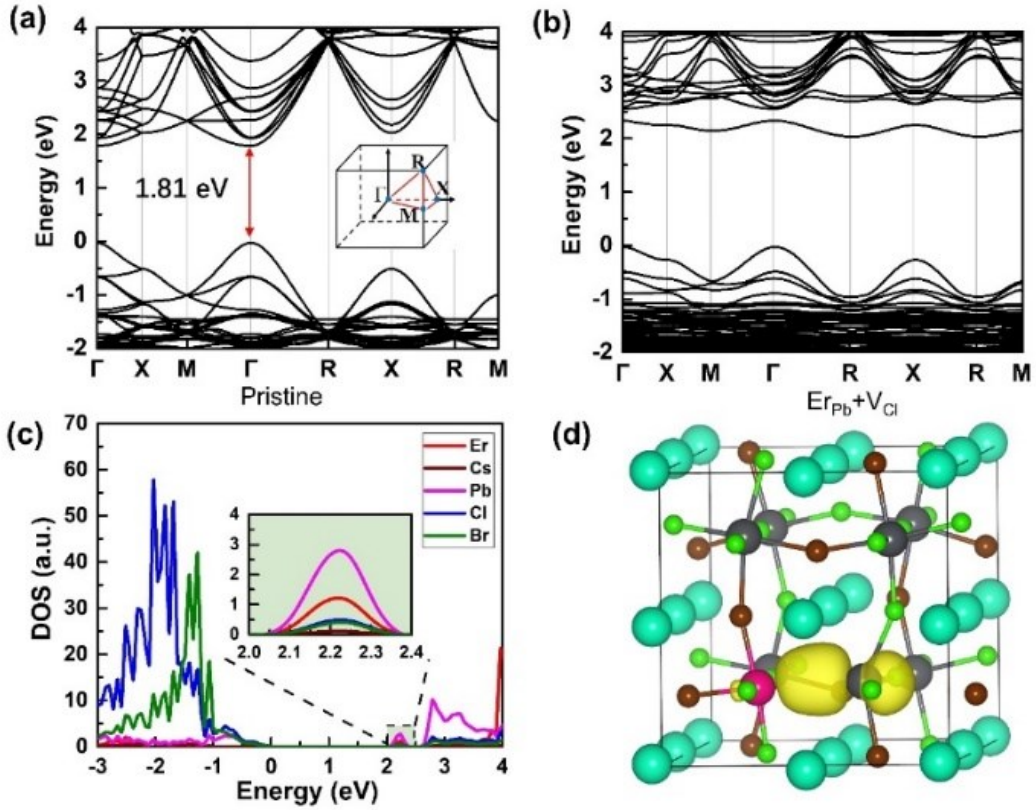


**Figure S7.** (a) Band structure of pristine $CsPbX_3$. (b) Band structure of Er:$CsPb(Br/Cl)_3$ with a Cl vacancy. (c) DOS of Er:$CsPb(Br/Cl)_3$ with a Cl vacancy. The inset shows that the main contribution of the defect level within the band gap is the Pb atom. (d) The charge distribution of defect state with isosurface value of 0.0030 eÅ$^{-3}$ (yellow).

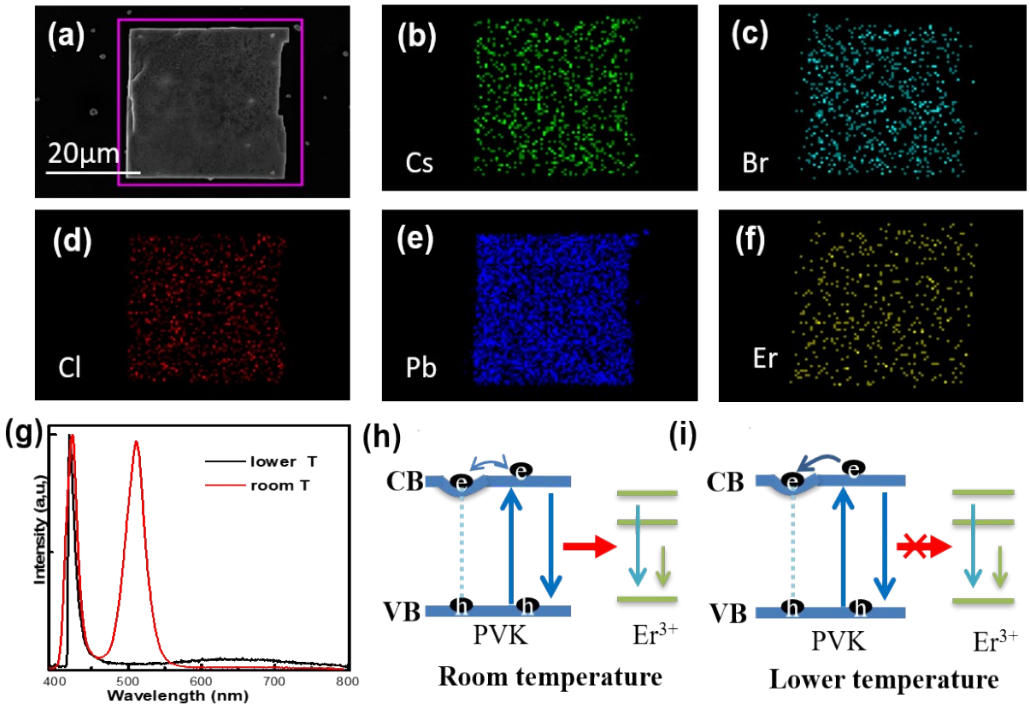


**Figure S8.** Material Characterization of Erbium-doped cesium lead halide perovskite microplates (Er:CsPb(Br/Cl)$_3$ MPs). (a) Scanning electron microscopy (SEM) image of the as grown MPs on silicon substrate. The typical MPs have the width of 10-40 μm. (b-f) Energy dispersive X-ray (EDX) mappings of the Cs, Pb, Cl, Br and Er elements, respectively. As can be seen the Cs, Pb, Cl, and Br elements uniformly distribute all over the plates, which confirms that the MPs are cesium lead halide PVK with a certain Cl/Br ratio. At room temperature, the emission of the doped sample shows two peaks which are locate at ~420 and ~520 nm and we respectively attribute these two peaks to the emission may from the PVK host and $Er^{3+}$ emission. At lower temperature, the $Er^{3+}$ emission disappear and a broad, low intensity red emission appear. This phenomenon represents the energy transfer from PVK host to $Er^{3+}$ are suppressed and self-trapped excitons are formed.[6,7]

**Table S2.** Fitting parameters of the dynamic curves for the FEs (450 nm) and STEs (700 nm) emissions.

| Peak (nm) | τ1 (ps) | A1(%) | τ2 (ps) | A2(%) | τ3 (ps) | A3(%) |
|---|---|---|---|---|---|---|
| 440 | 115 | 95.4 | 450 | 4.6 | - | - |
| 700 | 14 | 100.0 | 69 | 80.2 | 1400 | 19.8 |

## REFERENCES


1. Zhou, H.; Yuan, S.; Wang, X.; Xu, T.; Wang, X.; Li, H.; Zheng, W.; Fan, P.; Li, Y.; Sun, L.; Pan, A., *ACS Nano* 2017, **11,** 1189-1195.
2. Hu, X.; Zhou, H.; Jiang, Z.; Wang, X.; Yuan, S.; Lan, J.; Fu, Y.; Zhang, X.; Zheng, W.; Wang, X.; Zhu, X.; Liao, L.; Xu, G.; Jin, S.; Pan, A., *ACS Nano* 2017, **11,** 9869-9876.
3. Kohn, W.; Sham, L. J., *Physical Review* 1965, **140,** A1133-A1138.
4. Kresse, G.; Hafner, J., *Phys Rev B: Condens Matter* 1994, **49,** 14251-14269.
5. Pan, G.; Bai, X.; Yang, D.; Chen, X.; Jing, P.; Qu, S.; Zhang, L.; Zhou, D.; Zhu, J.; Xu, W.; Dong, B.; Song, H., *Nano Lett* 2017, **17,** 8005-8011.
6. Su, B.; Molokeev, M. S.; Xia, Z., *J Phys Chem Lett* 2020, **11,** 2510-2517.
7. Pinchetti, V.; Anand, A.; Akkerman, Q. A.; Sciacca, D.; Lorenzon, M.; Meinardi, F.; Fanciulli, M.; Manna, L.; Brovelli, S., *ACS Energy Lett* 2018, **4,** 85-93.